Debris flow: simulating the mitigation properties of vegetation

Debris flow: simulating the mitigation properties of vegetation

Alessandro Leonardi[1,2*], *Andrea* Pasqua[1,2], *Luca* Flammini[2], and *Marina* Pirulli[2]

[1]The University of Sheffield, Western Bank, S10 2TN Sheffield, UK
[2] Politecnico di Torino, Corso Duca degli Abruzzi 24, 10129 Torino, Italy

Abstract. Natural vegetation impacted by debris flows can act as an energy dissipator. This braking effect is similar to the one exerted by baffle arrays. However, this effect, and its potential for hazard mitigation, has been studied only marginally. In this work, we apply a depth-averaged model to reproduce scaled laboratory experiments of flow-forest interaction.

1 Introduction

Baffles are structural countermeasures used to mitigate the hazard associated to debris flows. The impact between a debris-flow front and baffles dissipates kinetic energy [1]. This has been observed to lead to a slow-down of the flow propagation. There are two beneficial effects associated to this. First, a flow with lower kinetic energy has also a lower entrainment potential [2]. Therefore, installing baffles early on in the catchment can reduce the overall size of events. Second, the impact on structures, and especially mitigation structures, is less momentous. Thus, baffles can be installed upstream of a barrier to improve the resilience of the overall mitigation system [3].

Much research has been devoted in developing frameworks for the evaluation of the effectiveness of baffles. In particular, laboratory studies have been conducted to find the optimal size, shape, number, spacing and arrangement of baffles [4,5]. This is often carried out as a function of the expected flow conditions [6,7]. Recently, numerical models are being employed as well, thanks to advances in complex 3D solvers for fluid and soil dynamics [8,9].

Baffles are typically built using traditional construction materials, such as steel or concrete, or using gabions. They therefore inherently come with embodied carbon. An interesting alternative to traditional baffles would be to use of natural elements as dissipators. Many tree species have strong trunks, which could withstand the impact of small debris flows [10,11]. An example of this is shown in Fig. 1. Trees could therefore have the same functions as traditional baffles, while at the same fulfilling other functions, such as slope stabilization, biodiversity conservation and carbon sequestration [12]. An additional complexity comes from the observation that any tree that is overturned or broken by the flow can be entrained as driftwood, increasing the mobilized volume. However, there is evidence that even entrained wood debris might help reducing runout [13].

Fig. 1. The deposit left by a debris flow next to a tree. In this case, the tree was able to withstand the impact. Courtesy of A. Booth [13].

It is difficult to quantify the mitigation effectiveness of any design than involves vegetation. Preliminary studies have been conducted by Vedrine *et al*. (2021) on snow avalanches [14], or Luong *et al*., (2020) on dry granular flows [15]. These studies have reported that vegetation can have a positive breaking effect, mobilizing friction and dispersing the flow laterally. However, they are still limited to a small number of trees, and an approach able to tackle the problem at the slope scale is still missing. In this respect, it appears vital to develop numerical frameworks able to simulate the scale of a natural forest. In this paper, we aim at filling this gap, by validating the use of a numerical framework to investigate forest-flow interaction. The flow of a granular mass, accelerated on an incline and impacting on a large sequence of obstacles, is reproduced. The obstacles have variable spacing, and are set to represent an idealized vegetated terrain. The preliminary geometrical setup presented here aims at back-analysing the experiments of Luong *et al*. (2020) [15], providing a benchmark for future studies.

* Corresponding author: alessandro.leonardi.ing@gmail.com; a.leonardi@sheffield.ac.uk

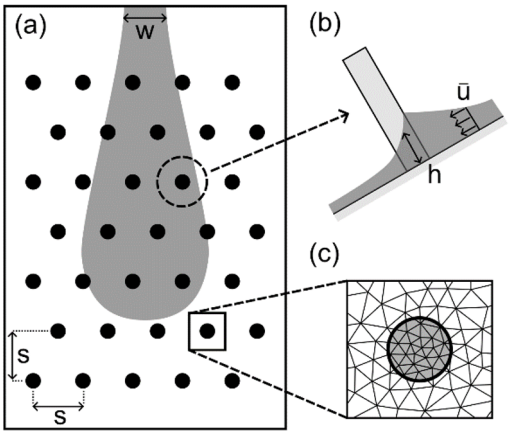

Fig. 2. Simulation setup: (a) planar view of the geometry; (b) representation of the interaction between flow and an obstacle; (c) mesh refinement in the proximity of an obstacle.

2 Methods

2.1 The benchmark experiments

The goal of this paper is to reproduce as close as possible the experiments of Luong *et al*., (2020) [15]. Their setup is illustrated in Fig. 2(a). The flow was generated on an incline with constant slope *θ,* adjustable between 28° and 40°. The surface was a cork board, which has relatively low roughness. The employed grains were glass beads, of mean diameter d=0.3 mm and density 2500kg/m^3. They were released through a double-gate system, lifted manually. Once lifted, the gate had a fixed height H, which could be adjusted between 13 and 43mm, and a fixed width W=97mm. A total of 5 kg of spheres were released during each realization.

In the experiments, the plane had been modified to accommodate a series of cylindrical obstacles, i.e. the model trees. The obstacles had constant diameter $D = 20$ mm, and variable spacing S. The spacing analysed were 40, 60, and 80 mm. The obstacles were arranged on a regular hexagonal (honeycomb) pattern.

2.2 Numerical simulation setup

The experiments are back-analysed based on a set of simplifications. The granular material is simulated as an equivalent continuum, with homogeneous properties. Therefore, any area where the flow loses its dense state cannot be accurately simulated. This is for example the front, where single beads might detach from the main flow body. It is also assumed that the flow is shallow, and that velocity has a negligible component in the direction orthogonal to the slope. This last hypothesis is clearly challenged by the presence of the obstacles, as flow is bound to run up at impact, see Fig. 2(b). However, as will be clearer in the following section, a good approximation of the macroscopic characteristics of the flow can nevertheless be obtained.

As a consequence of these simplification, one can safely assume that the flow resistance is governed by a single rheological law. Due to its popularity, we employ the rheology proposed by Pouliquen (1999) [16], in which resistance is frictional. This rheology prescribes a non-constant basal friction coefficient, which increases with the Froude number Fr as:

$$\mu = \mu_s + \frac{\mu_d - \mu_s}{\frac{\beta h}{L d \mathrm{Fr}^2} + 1}. \quad (1)$$

Here, μ_s is the base friction coefficient, corresponding to the angle of incipient motion, and μ_d is the secondary friction coefficient, corresponding to the maximum slope where steady conditions can be achieved. The two parameters β and L are a function of the material and of the flow configuration, and h is the flow height (see Fig 2b). The three-dimensional form of this rheology is the well-known $\mu(I)$ rheology [17].

The conservation of mass and momentum are solved using a set of depth-averaged equations, discretized with a finite-volume approach. The solution is performed with the software RASH3D, which has been validated multiple times on similar conditions [18,19].

The model trees are reproduced as local variations of the topographical surface, which is elsewhere planar. Overall, the plane is discretized with a mesh size of 0.005 m. The mesh is locally refined around every tree, as shown on Fig. 2(c). The gate is simulated as an inlet boundary, with constant influx. On all other boundaries, an outlet condition is imposed.

3 Numerical results

3.1 Calibration

The rheology is calibrated via a trial-and-error procedure. The starting point is the set of numerical parameters proposed by Luong et al. (2020). The main calibration goal is to reproduce as close as possible the propagation speed, measured as the evolution of the flow length L as a function of time. The best fit is obtained with $\mu_s = 0.41$, $\mu_d = 1.47$, $L = 0.025$, and $\beta = 0.6$. Of these, only β differs significantly from typical literature values for glass beads. A possible reason for this is the bed material in the experiments (a cork board). Its roughness is probably lower than the one employed if a layer of glass beads had been glued to the bed.

3.2 Flow shape and braking effect

We report two set of observations. Firstly, a qualitative assessment of the influence of the obstacles/trees on the flow shape. Although the flow-obstacle interaction is simplified due to the depth-averaging procedure, the flow shape is strikingly similar to the one reported in the experiments. As an example, Fig. 3 reports the aerial view of the plane at 1.5 s, for two different obstacle configurations. The figure shows the comparison between the flow shape in experiments and the corresponding numerical simulations. Although discrepancies are evident, the depth-averaged model is able to capture the flow partition that occurs around each obstacle with remarkable accuracy.

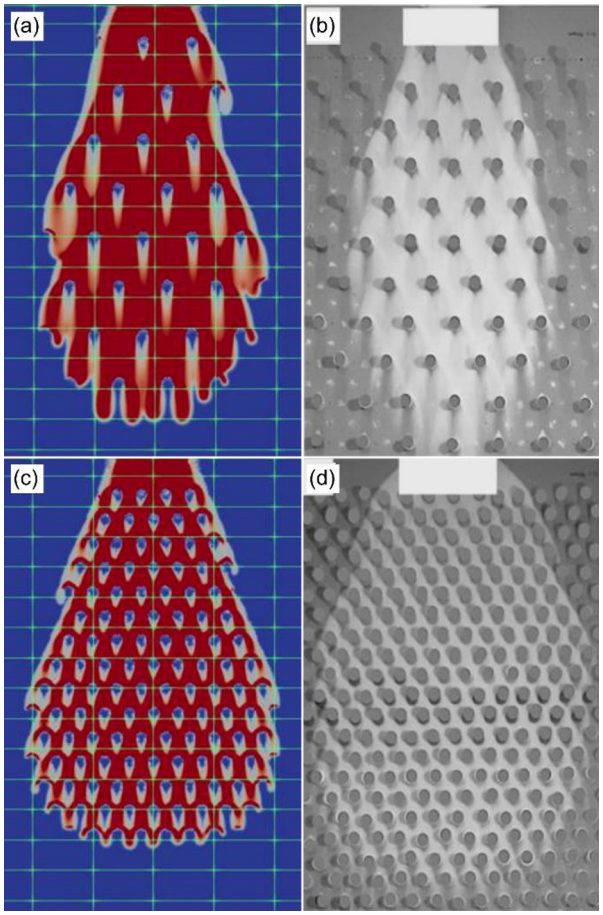

Fig. 3. Comparison between experiments and simulation, areal view of the plane, captured 1.5 s after release. Images on the left are visualization of the simulation. The area highlighted in red is where the flow thickness is larger than d. On the right are pictures taken from Luong *et al*. (2020) [15]. The panels on the top row (a,b) report the results with an obstacle spacing $S = 0.08$ m, while the bottom row (c,d) shows the results with $S = 0.04$ m. In this setup the incline slope is $\theta = 30°$, and the gate height is $H = 24$ mm.

To test the capability to reproduce the braking effect of the obstacle, the time-evolution of the flow shape is also measured. This is juxtaposed with the equivalent observations in the experiment. The result of this comparison is show on Fig. 4. Panel (a) shows the total length of the flow L, measured as the distance between the flow front and the inlet. The simulations yield flows that are generally faster in the initial stage, although the difference smoothens at later stages. This is probably due to difficulties in modelling accurately the type of inlet used in the experiments. However, the braking effect of the obstacles is reproduced satisfactorily: Denser obstacles distribution slow down the flow considerably, and speed up the transient phase.

Panel (b) illustrates how the model forest induces a lateral expansion of the flowing material. Once more, the simulations are able to reproduce accurately the influence of the obstacles. Denser model forests induce a wider lateral expansion. This implies a more intense mobilization of bed friction. This can be speculated to aid in slowing down the flow propagation.

4 Conclusions

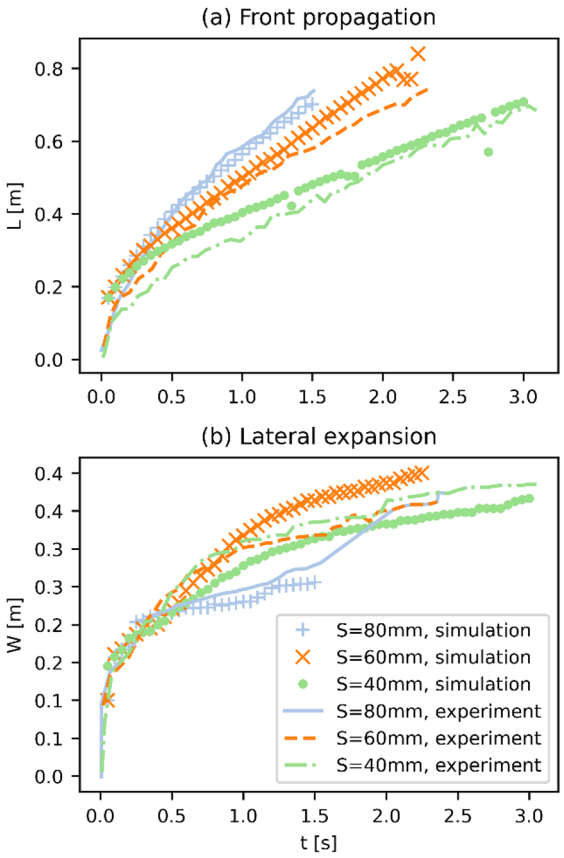

Fig. 4. Influence of the obstacles on (a) the front propagation, and (b) on the lateral spread-out of the mass. The figure also compares simulations and experiments. Results are for the setup with incline slope is $\theta = 30°$, and gate height $H = 24$ mm.

It is apparent that the obstacles have two concurrent effects. Firstly, each obstacle dissipates energy when impacted. Thus, denser forests might be effective at reducing entrainment and mitigating the related hazard.

Secondly, denser forests induce a lateral spread of the flow. This effects, which had been already observed and described by Luong *et al*., (2020) [15] has been reproduced very well by the simulations. This is promising, as the simulations allow for much more flexibility in testing different tree patterns and size distributions.

Both effects, however, are valid under the hypothesis of the trees being able to withstand the impact without being overturned. This might be likely for small debris flows, but is unforeseeable for events with medium or large magnitude. However, there is field evidence [13] that even overturned trees, once entrained by the flow, would aid in slowing down the flow propagation. This effect remains to be studied with more detail.

References

1. A. Leonardi, M. Pirulli, C.-Y. Yune, C.E. Choi, *Study of the influence of baffles on an artificial debris flow through back-analysis simulations*, in Second JTC1 Workshop on Triggering and Propagation of Rapid Flow-like Landslides, (2018).

2. F. Frank, B.W. McArdell, C. Huggel, A. Vieli, *Natural Hazards and Earth System Sciences*, *15*(11), 2569–2583 (2015).
3. C.E. Choi, C.W.W. Ng, D. Song, J.H.S. Kwan, H.Y.K. Shiu, K.K.S. Ho, R.C.H. Koo, *Canadian Geotechnical Journal*, **51**(5), 540–553 (2014).
4. F. Wang, X. Chen, J. Chen, Y. You, *Engineering Geology*, **220**, 43–51 (2017).
5. H. Yang, M.E. Haque, K. Song, *Physics of Fluids*, **33**(5) (2021).
6. A. Leonardi, S.R. Goodwin, M. Pirulli, *Acta Geotechnica*, **14**(6), 1949–1963 (2019).
7. A. Pasqua, A. Leonardi, M. Pirulli, *Computers and Geotechnics*, **104879** (2022).
8. X. Li, Q. Yan, S. Zhao, Y. Luo, Y. Wu, D. Wang, *Landslides*, **17**(5), 1129–1143 (2020).
9. S. Li, C. Peng, W. Wu, S. Wang, X. Chen, J. Chen, G.G.D. Zhou, B.K. Chitneedi, *Landslides*, **17**(9), 2099–2111 (2020).
10. X. Zhang, J.A. Knappett, A.K. Leung, M. Ciantia, T. Liang, F. Danjon, *Plant and Soil*, **456**(1–2), 289–305 (2020).
11. K. Jin, J. Chen, X. Chen, W. Zhao, G. Si, X. Gong, *Journal of Mountain Science*, **18**(7), 1874–1885 (2021).
12. S. Wang, X. Meng, G. Chen, P. Guo, M. Xiong, R. Zeng, *Geomorphology*, **282**, 64–73 (2017).
13. A.M. Booth, C. Sifford, B. Vascik, C. Siebert, B. Buma, *Earth Surface Processes and Landforms*, **45**(7), 1555–1568 (2020).
14. L. Védrine, X. Li, J. Gaume, *Natural Hazards and Earth System Sciences*, **22**(3), 1015–1028 (2022).
15. T.H. Luong, J.L. Baker, I. Einav, *Granular Matter*, **22**(1), 1–10. (2020).
16. O. Pouliquen, *Physics of Fluids*, **11**(3), 542 (1999).
17. P. Jop, Y. Forterre, O. Pouliquen, *Nature*, **441**(7094), 727–730 (2006).
18. A. Leonardi, M. Pirulli, M. Barbero, F. Barpi, M. Borri-Brunetto, O. Pallara, C. Scavia, V. Segor, Environmental and Engineering. Geosciences **27**(2), 195–212 (2021).
19. M. Pirulli, M.O. Bristeau, A. Mangeney, C. Scavia, Environmental Modeling and Software **22**(10), 1437–1454 (2007).